PHYSICAL REVIEW B **87**, 235439 (2013)

Giant photocurrents in a Dirac fermion system at cyclotron resonance

P. Olbrich,[1] C. Zoth,[1] P. Vierling,[1] K.-M. Dantscher,[1] G. V. Budkin,[2] S. A. Tarasenko,[2] V. V. Bel'kov,[2] D. A. Kozlov,[3]
Z. D. Kvon,[3] N. N. Mikhailov,[3] S. A. Dvoretsky,[3] and S. D. Ganichev[1]
[1]*Terahertz Center, University of Regensburg, 93040 Regensburg, Germany*
[2]*A.F. Ioffe Physical-Technical Institute, Russian Academy of Sciences, 194021 St. Petersburg, Russia*
[3]*Institute of Semiconductor Physics, Novosibirsk, Russia*
(Received 26 March 2013; published 28 June 2013)

We report on the observation of the giant photocurrents in HgTe/HgCdTe quantum well (QW) of critical thickness at which a Dirac spectrum emerges. At an exciting QW of 6.6 nm width by terahertz (THz) radiation and sweeping magnetic field we detected a resonant photocurrent. Remarkably, the position of the resonance can be tuned from negative (−0.4 T) to positive (up to 1.2 T) magnetic fields by means of optical doping. The photocurrent data, accompanied by measurements of radiation transmission as well as Shubnikov–de Haas and quantum Hall effects, prove that the photocurrent is caused by cyclotron resonance in a Dirac fermion system, which allows us to obtain the effective electron velocity $v \approx 7.2 \times 10^5$ m/s. We develop a microscopic theory of the effect and show that the inherent spin-dependent asymmetry of light-matter coupling in the system of Dirac fermions causes the electric current to flow.

DOI: 10.1103/PhysRevB.87.235439 PACS number(s): 73.21.Fg, 72.25.Fe, 78.67.De, 73.63.Hs

I. INTRODUCTION

The electron dc transport in semiconductor systems with massless Dirac fermions has recently moved into the focus of modern research yielding challenging fundamental concepts as well as holding a great potential for applications.[1–3] The linear energy spectrum allows the observation of quantum kinetic effects and, on the other hand, gives rise to a new class of phenomena absent in materials with parabolic dispersion. The massless Dirac fermions are realized in graphene,[4] at surface states of bulk topological insulators (TIs),[1–3,5] in edge channels of two-dimensional TIs,[6] as well as in HgTe/HgCdTe QWs of critical thickness.[7–9] In the latter case and TIs, the linear energy spectrum is formed by strong spin-orbit interaction which locks the orbital motion of carriers with their spins. The interest in Dirac fermions in such materials resulted in theoretical consideration and observation of such fundamental physical phenomena as the quantum spin Hall effect,[6,7,10–12] quantum Hall effect (QHE) on topological surface states,[13] magnetoelectric effect,[14,15] and quantum interference effects.[16–21] Considerable attention has also been given to the *nonlinear* high frequency (HF) transport phenomena. A plethora of such effects has been treated theoretically, including photogalvanics in TI systems,[22–25] second harmonic generation (SHG),[26] as well as radiation-induced QHE[27] and topological states.[28] While a great number of proposals have been published in the last two years, the number of experiments on the topic is limited so far by a few publications reporting the observation of SHG and photogalvanic effects in three-dimensional (3D) TIs induced by near infrared radiation.[26,29–31]

Here we report on the observation of a dc current excited by THz radiation in HgTe/HgCdTe QWs of critical thickness. We show that the current at cyclotron resonance (CR) is a few orders of magnitude higher than THz radiation excited photocurrents detected in other nonmagnetic QW structures. Due to the linear dispersion of massless Dirac fermions, the CR position is tuned by the variation of carrier density applying optical doping. The microscopic origin of the current is discussed in terms of the cyclotron motion, spin-dependent scattering, and Zeeman splitting. We show that the current is spin polarized, its large magnitude comes from constructively contributing three factors: strong spin-orbit coupling, large g factor in HgTe/HgCdTe QWs, and efficient radiation absorption at CR.

II. EXPERIMENT

The experiments are carried out on (013)-oriented HgTe/$\mathrm{Hg_{0.3}Cd_{0.7}Te}$ QWs.[32] Single QW samples with widths L_w of 6.6 and 21 nm and mobilities about 10^5 cm^2/(V s) at $T = 4.2$ K are investigated. The structures cross section is shown in Fig. 1(a). Eight ohmic contacts have been prepared at the corners and in the middle of the edges of 5×5 mm^2 samples. Magnetotransport measurements show well pronounced Shubnikov–de Haas oscillations and QHE plateaus, see Fig. 1(c). To achieve a controllable variation of the carrier density we applied optical doping using the persistent photoconductivity effect well known for HgTe/HgCdTe QWs.[9,33,34] We illuminate the sample by red light emitting diode operating at a wavelength of 630 nm for a time t_i resulting in a change of the carrier density (type) which could be restored by heating the sample above $T \approx 150$ K. The carrier densities measured for different t_i used in the experiments are given in Table I.

For photocurrent excitation we apply a cw $\mathrm{CH_3OH}$ laser emitting a radiation with frequency $f = 2.54$ THz (wavelength $\lambda = 118$ μm).[35] The incident power $P \approx 10$ mW is modulated at 800 Hz by an optical chopper. The radiation at normal incidence is focused in a spot of about 1.5 mm diameter at the center of the sample. The spatial beam distribution has an almost Gaussian profile which is measured by a pyroelectric camera.[36] Right (σ^+) and left (σ^-) handed circularly polarized light is obtained by a $\lambda/4$ plate. The experimental geometry is sketched in Fig. 1(b). In (013)-oriented QWs, excitation by normally incident THz radiation results in a photogalvanic current even at $B_z = 0$,[37–39] for details see the Appendix. Owing to low symmetry of QW (C_1

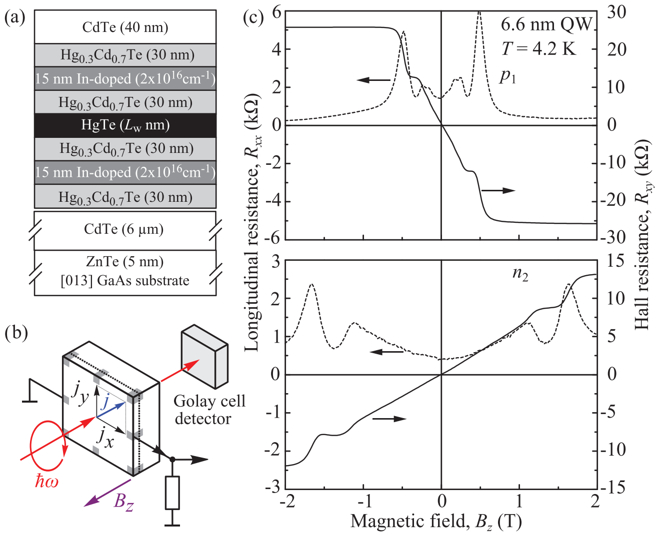

FIG. 1. (Color online) (a) Cross section of the investigated structures. (b) Experimental setup used for the photocurrent and transmission measurements. (c) Magnetotransport data obtained in the van der Pauw geometry for 6.6 nm HgTe/HgCdTe QW sample without (top) and with (bottom) optical doping. The change of slope in the Hall signal indicates that initially the p-type sample becomes n-type due to optical doping.

point group), the photocurrent has no predefined direction and its magnitude $j = \sqrt{j_x^2 + j_y^2}$ can be deduced by measuring the signals along two orthogonal directions.[40] The current-induced photovoltages $U_{x,y}$ are picked up across a 1 MΩ load resistor applying lock-in technique. The magnetic field B_z up to 4 T is applied normal to the QW plane. The photocurrent studies are accompanied by optical transmission, see Fig. 1(b), and magnetotransport experiments.

We start with the data obtained on the 6.6 nm QW, which should have a close to linear dispersion.[9,21] Exciting the sample with right-handed circularly polarized radiation and sweeping magnetic field we observed a strong resonant photosignal at $B_c = -0.42$ T, see Fig. 2. The signal at the resonance is more than two orders of magnitude higher than that detected at $B_z = 0$. By changing the carrier type from a hole to an electron the resonance jumps from negative to positive B_z and moves towards higher field, now being for the electron density $n_1 \approx 2 \times p_1$ at $B_c = +0.69$ T. Remarkably, at further increase in the electron density, the resonance position drifts to even higher B_c, being 1.2 T for $n_2 \approx 3 \times n_1$, see Fig. 2. For a fixed helicity of circularly polarized radiation, the photosignal has a resonance for one magnetic field polarity only. Switching the radiation helicity from σ^+ to σ^- changes the current sign and mirrors the results with respect to the magnetic field polarity (not shown). For linearly polarized radiation being the superposition of σ^+ and σ^- photons, the resonant photovoltage is observed for both magnetic field polarities, as shown for p-type conductivity in the inset in Fig. 2. We stress that the resonant photosignal changes the sign upon reversing the magnetic field direction. The above behavior is observed for the temperature range from 4.2 up to 150 K. The resonances are detected in the transmission measurements as well. The data for different carrier densities (type) are shown in Fig. 3 demonstrating a good correlation between the positions of the dip in the transmissivity and the resonant photosignal. The values of the momentum relaxation time τ_p obtained from the width of CR are given in Table I.

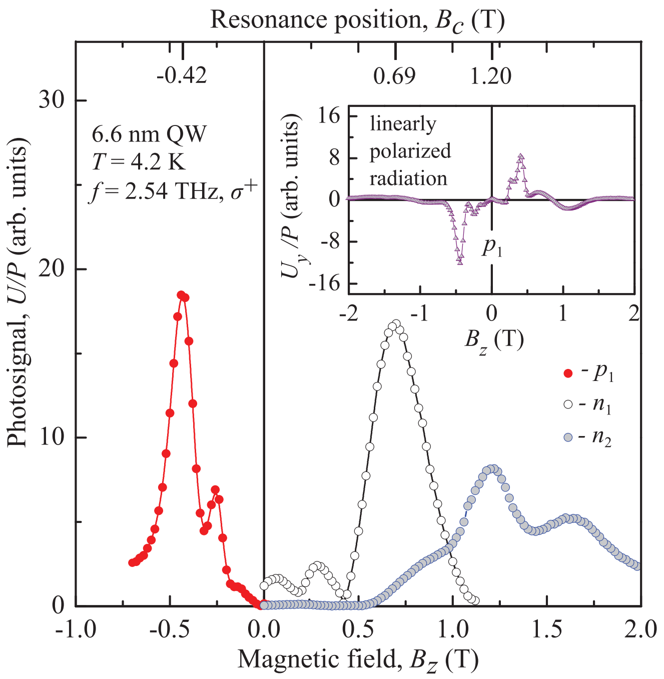

FIG. 2. (Color online) Signal normalized by the radiation power U/P excited by σ^+ radiation vs B_z. The data are shown for magnetic fields lower than the full quantization limit.[41] The inset shows the photovoltage measured along the y-direction U_y for linearly polarized light.

TABLE I. Sample parameters measured at $T = 4.2$ K. The values of τ_p are obtained from the CR width, see Fig. 3.

	L_w (nm)	τ_i (s)	Density (cm$^{-2}10^{10}$)	E_F (meV)	τ_p (ps)
p_1	6.6	–	1.5	15	0.19
n_1	6.6	15	3.4	21	0.19
n_2	6.6	80	11.0	39	0.32
n_3	21.0	–	18.0	15	1.6
n_4	21.0	80	24.0	21	2.35

Resonant photosignals are also detected for the 21 nm QWs, a structure characterized by a nearly parabolic dispersion. Photosignals (see Fig. 4, left panel) and transmission measurements (see Fig. 3) clearly show that the resonance position in these QWs is shifted to much higher magnetic fields $B_c \approx 3$ T. Furthermore, the resonance field now only slightly depends on the carrier density.

The observed coincidence of peak positions in the photosignal and transmissivity unambiguously proves that the resonant current is caused by CR.[42] This is also supported by the fact that for a fixed radiation helicity the resonances in the photocurrent and transmissivity are detected for one polarity of magnetic field only. The striking fact is that, depending on optical doping, the resonance for QWs with $L_w = 6.6$ nm is detected for negative as well as for positive magnetic field and its peak position drastically depends on the Fermi level. These

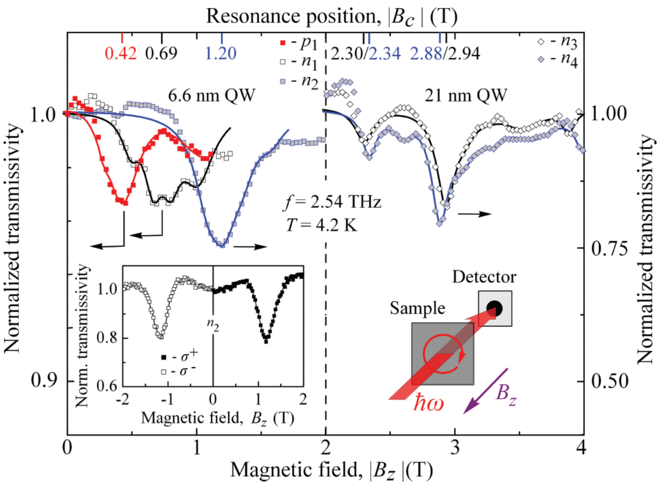

FIG. 3. (Color online) Transmissivity of circularly polarized light measured as a function of the magnetic field modulus $|B_z|$ and normalized by the zero-field transmissivity. Full lines are fits by a superposition of Lorentz functions. The inset shows the data obtained for σ^+ and σ^- light for the $L_w = 6.6$ nm samples.

results are in agreement with Ref. 9 which concludes that the energy dispersion in similar structures is close to linear. Such an electron spectrum lacks the band gap and, therefore, allows an easy transition from n- to p-type conductivity, as proved in transport and CR experiments, see Figs. 1–3. Furthermore, recent study of gated Hall bar 6.6 nm QWs samples prepared from the same batch, as samples studied here, manifests weak localization effects even in the vicinity of a Dirac point giving additional proof for existence of gapless dispersion in these QWs.[21] As a matter of fact, the cyclotron frequency in a system with linear dispersion depends strongly on the Fermi energy—a characteristic behavior observed in our 6.6 nm sample. Indeed, the cyclotron frequency is described by the well known expression $|\omega_c| = |eB_z|/m_c c$, where e is the carrier charge, c is the speed of light, and m_c is the effective cyclotron mass at the Fermi energy. The latter, given by $m_c = p_F/(dE_F/dp_F)$, with p_F being the Fermi momentum, yields $m_c = E_F/v^2$ for a system with linear dispersion characterized by a constant velocity v. Taking $E_F = \sqrt{2\pi n}(\hbar v)$ into account, we obtain for the CR position $|B_c| = \sqrt{2\pi n}(c\hbar\omega)/|ev|$. From the resonance positions measured for electron densities n_1 and n_2 (Fig. 2) we find that the electron Fermi velocity is almost constant, being equal to 7.2×10^5 m/s. The value is in a good agreement with the electron velocity for 2D Dirac fermions in HgTe/HgCdTe QWs of critical thickness $v = 6.3 \times 10^5$ m/s, obtained from the energy spectrum calculated in Ref. 8. The hole velocity, deduced from our data for the density p_1, is also close to this value (7.5×10^5 m/s). Note that the obtained values are close to the carrier velocity in graphene[4] (10^6 m/s). The substantially higher resonance field in 21 nm QWs as well as the observed weak dependence of its position on the electron density correspond to the CR behavior in HgTe/HgCdTe QWs characterized by a nearly parabolic dispersion with large Zeeman splitting.[33,34,43–46]

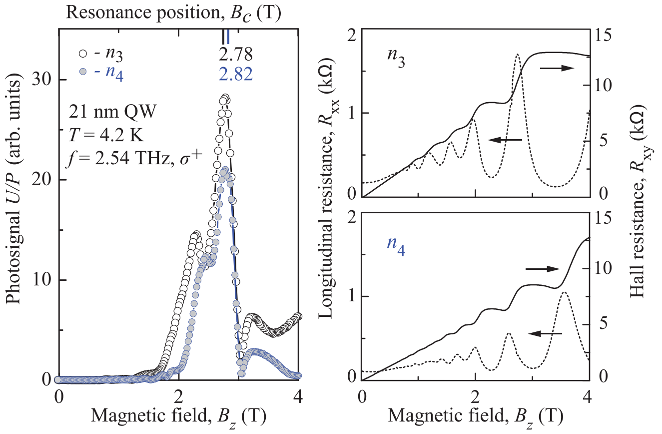

FIG. 4. (Color online) Left panel: Magnetic field dependence of the signal U/P excited by σ^+ light in the 21 nm sample. Right panel shows the magnetotransport data.

III. DISCUSSION AND MICROSCOPIC MODEL

Now we turn to the microscopic origin of the current generation at cyclotron resonance. For linearly polarized radiation the resonant photosignal changes a sign upon switching the magnetic field polarity, see the inset in Fig. 2. This is in contrast to the absorption and photoconductivity[9] which are even in the field. Moreover, the observed photosignal at cyclotron resonance, e.g., for the density p_1, is about two orders of magnitude larger than that measured at zero magnetic field, see the inset in Figs. 2 and 6(a). This increase in the signal magnitude is much higher than the increase of radiation absorption given by $(\omega_c \tau_p)^2$ being about eight for the same density. The latter was estimated from the width of CR, see Fig. 3. Both observations suggest that the photocurrent detected at the cyclotron resonance is not merely the current at zero field enhanced by cyclotron resonance but is of another microscopic root. The fact that the current is excited at normal incidence of radiation implies that it is inherently related to asymmetry of carrier relaxation (excitation) in $\boldsymbol{k}$ space in (013)-oriented QWs of low spatial symmetry.[47] In HgTe/HgCdTe QWs of critical thickness, where the subband structure is formed by spin-orbit coupling, the most likely candidate responsible for the microscopic origin of the asymmetry is spin-dependent scattering. The latter is a known fact for other III-V and II-VI heterostructures.[48–51] We consider the resonant absorption of THz radiation, which leads to the strong electron (hole) gas heating. The resulting steady-state nonequilibrium carrier distribution is formed by the energy gain due to the radiation absorption, electron-electron collisions thermalizing the electron gas, and the energy loss due to emission of phonons. The matrix element of electron scattering by phonon contains asymmetric spin-dependent terms (odd in the electron wave vector), which are similar to the Rashba and Dresselhaus spin-orbit terms in the energy dispersion.[52] Below we present the $\boldsymbol{k}\cdot\boldsymbol{p}$ calculation of the matrix elements of electron-phonon interaction in HgTe/CdHgTe QWs with linear dispersion and show that the interaction is substantially spin dependent. Due to the spin-dependent part of the electron-phonon interaction, the energy relaxation of carriers in the spin cones is asymmetric and the relaxation rates for positive and negative wave vectors, say in the x direction, are different.[53] The asymmetry causes imbalance in the carrier distribution in $\boldsymbol{k}$ space and,

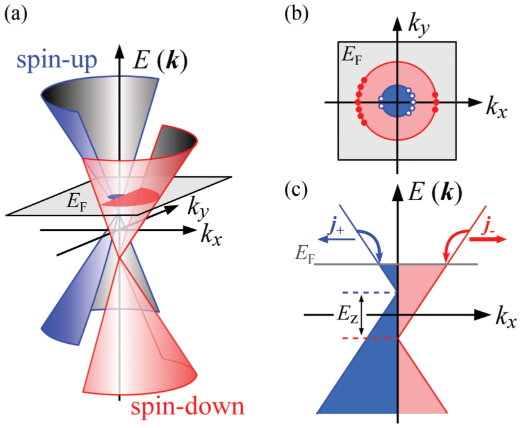

FIG. 5. (Color) Microscopic model. (a) Energy dispersion with spin-up (left, blue) and spin-down (right, red) cones shifted due to Zeeman effect to higher and lower energies, respectively. (b) Nonequilibrium carrier distribution at Fermi energy caused by the spin-dependent scattering. Full and open circles sketch the electron distribution in $\boldsymbol{k}$ space. (c) Energy relaxation of an electron gas heated as a result of the radiation absorption. Due to the spin-dependent scattering, the relaxation rates for electrons with positive and negative $\boldsymbol{k}$ are different. Bent arrows show schematically a predominant energy relaxation in the spin-up (left) and spin-down (right) cones. The scattering asymmetry within each cone results in the oppositely directed fluxes $\boldsymbol{j}_+$ and $\boldsymbol{j}_-$ shown by horizontal arrows. As due to the Zeeman effect the spin-down cone is larger populated, the flux $\boldsymbol{j}_-$ is stronger than $\boldsymbol{j}_+$ and a dc electric current emerges.

hence, electron fluxes, see Fig. 5(b). The latter have opposite directions in the spin-up and spin-down cones. As, besides the cyclotron motion, the magnetic field splits the spin cones due to the Zeeman effect, one of the cones is preferentially populated compared to the other. Consequently, the fluxes in the spin cones are unbalanced, and a net electric current emerges. This process is sketched in Fig. 5(c) and, besides the linear dispersion, is alike that known for other nonmagnetic QW structures.[48,49] Obviously the current magnitude is proportional to the radiation absorption, the strength of spin-orbit coupling, and the Zeeman splitting. The absorption is strongly enhanced in HgTe/HgCdTe QWs at the CR condition, resulting in the giant photocurrent observed in the experiments. While the models of the current formation for QWs with linear and parabolic dispersions are similar, the position of CR and its behavior upon variation of the Fermi energy are different. In particular, for a fixed radiation frequency, the magnetic field corresponding to CR is independent of the carrier density in QWs with parabolic spectrum. By contrast, for QWs with linear spectrum, it drastically depends on the carrier density and, for circularly polarized light, may even change its polarity in the same structure when the Fermi level crosses the neutrality point.

IV. MICROSCOPIC THEORY

Following the model above, we now develop the quasi-classical theory of the effect. We describe the electron states in HgTe/CdHgTe quantum wells in the isotropic $\boldsymbol{k}\cdot\boldsymbol{p}$ model following Ref. 7. The Dirac cones in the QW of critical width are formed from the four states

$$\begin{aligned}|E1,+1/2\rangle &= f_1(z)|\Gamma_6,+1/2\rangle + f_4(z)|\Gamma_8,+1/2\rangle,\\ |H1,+3/2\rangle &= f_3(z)|\Gamma_8,+3/2\rangle,\\ |E1,-1/2\rangle &= f_1(z)|\Gamma_6,-1/2\rangle + f_4(z)|\Gamma_8,-1/2\rangle,\\ |H1,-3/2\rangle &= f_3(z)|\Gamma_8,-3/2\rangle,\end{aligned} \tag{1}$$

which are degenerate at $\boldsymbol{k}=0$, with $\boldsymbol{k}$ being the in-plane wave vector. Here $f_1(z)$, $f_3(z)$, and $f_4(z)$ are the envelope functions, which can be chosen real, z is the growth direction, $|\Gamma_6,\pm1/2\rangle$, $|\Gamma_8,\pm1/2\rangle$, and $|\Gamma_8,\pm3/2\rangle$ are the basis functions of the Γ_6 and Γ_8 bands. At $\boldsymbol{k}\neq 0$, the states (1) are coupled that is described by the effective Hamiltonian

$$H = \begin{pmatrix} 0 & iAk_+ & 0 & 0\\ -iAk_- & 0 & 0 & 0\\ 0 & 0 & 0 & -iAk_-\\ 0 & 0 & iAk_+ & 0\end{pmatrix}, \tag{2}$$

where A is the (real) constant describing the in-plane velocity $A \approx (P/\sqrt{2})\int f_1(z)f_3(z)dz$, $P = i(\hbar/m_0)\langle S|p_z|Z\rangle$ is the Kane matrix element, and $k_\pm = k_x \pm ik_y$. The sign of A depends on the sign of $f_3(z)$, we take $A>0$. Solution of the Schrödinger equation with the Hamiltonian (2) for positive energy $\varepsilon_k = Ak$ yields two functions:

$$\begin{aligned}\psi_{+,\boldsymbol{k}} &= \frac{\exp(i\boldsymbol{k}\cdot\boldsymbol{\rho})}{\sqrt{2}}\begin{pmatrix}1\\ -i\exp(-i\varphi)\\ 0\\ 0\end{pmatrix},\\ \psi_{-,\boldsymbol{k}} &= \frac{\exp(i\boldsymbol{k}\cdot\boldsymbol{\rho})}{\sqrt{2}}\begin{pmatrix}0\\ 0\\ 1\\ i\exp(i\varphi)\end{pmatrix},\end{aligned} \tag{3}$$

where $\varphi = \arctan(k_y/k_x)$ is the polar angle of the wave vector.

We consider (013)-grown QWs and chose the coordinate frame $x\parallel[100]$, $y\parallel[03\bar{1}]$, and $z\parallel[013]$. In such a coordinate system, the basis functions of the Γ_6 and Γ_8 bands can be presented in the form

$$|\Gamma_6,+1/2\rangle = S\uparrow,\quad |\Gamma_6,-1/2\rangle = S\downarrow, \tag{4}$$

$$\begin{aligned}|\Gamma_8,+3/2\rangle &= -\frac{X' + i(Y'\cos\theta - Z'\sin\theta)}{\sqrt{2}}\uparrow,\\ |\Gamma_8,+1/2\rangle &= \sqrt{\frac{2}{3}}(Z'\cos\theta + Y'\sin\theta)\uparrow\\ &\quad -\frac{X' + i(Y'\cos\theta - Z'\sin\theta)}{\sqrt{6}}\downarrow,\\ |\Gamma_8,-1/2\rangle &= \sqrt{\frac{2}{3}}(Z'\cos\theta + Y'\sin\theta)\downarrow\\ &\quad +\frac{X' - i(Y'\cos\theta - Z'\sin\theta)}{\sqrt{6}}\uparrow,\\ |\Gamma_8,-3/2\rangle &= \frac{X' - i(Y'\cos\theta - Z'\sin\theta)}{\sqrt{2}}\downarrow,\end{aligned} \tag{5}$$

where S, X', Y', and Z' are the Bloch amplitude of the Γ_6 and Γ_8 bands, respectively, referred to the cubic axes $x' \| [100]$, $y' \| [010]$, and $z' \| [001]$, $\theta \approx 18.4^\circ$ is the angle between the [001] and [013] axes, and the symbols $\uparrow$ and $\downarrow$ denote the spin projections $+1/2$ and $-1/2$ onto the z axis, respectively.

The deformation interaction of electrons with acoustic phonons in zinc-blende-type crystals has both intraband and interband contributions.[54–56] The matrix elements of strain-induced interband coupling are given by $V_{S,X'} = \Xi_{cv} u_{y'z'}$, $V_{S,Y'} = \Xi_{cv} u_{x'y'}$, $V_{S,Z'} = \Xi_{cv} u_{x'y'}$, where Ξ_{cv} is the interband constant of the deformation potential and $u_{\alpha\beta}$ are the strain-tensor components used here in the primed coordinate system. Note that $\Xi_{cv} \neq 0$ in noncentrosymmetric crystals only. The matrix elements of strain-induced intraband interaction are taken in the form $V_{S,S} = \Xi_c \,\mathrm{Tr}\, u_{\alpha\beta}$, $V_{X',X'} = V_{Y',Y'} = V_{Z',Z'} = \Xi_v \,\mathrm{Tr}\, u_{\alpha\beta}$, where Ξ_c and Ξ_v are the deformation-potential constants ($\Xi_v = a$ in the Bir-Pikus notation,[57] the constants b and d are neglected for simplicity). Accordingly, the Hamiltonian of electron-phonon interaction in the basis of functions (4) and (5) has the form

$$V = \begin{pmatrix} V_c & V_{cv} \\ V_{cv}^\dagger & V_v \end{pmatrix}, \tag{6}$$

where $V_c = \Xi_c (\mathrm{Tr}\, u_{\alpha\beta}) I_2$, $V_v = \Xi_v (\mathrm{Tr}\, u_{\alpha\beta}) I_4$, and I_2 and I_4 are the identity matrices 2×2 and 4×4, respectively,

$$V_{cv}^\dagger = \Xi_{cv} \begin{pmatrix} -\frac{(u_{yz} - i u_{xz}) \cos 2\theta + (u_{zz}/2 - u_{yy}/2 + i u_{xy}) \sin 2\theta}{\sqrt{2}} & 0 \\ \sqrt{\frac{2}{3}} (u_{xy} \cos 2\theta + u_{xz} \sin 2\theta) & -\frac{(u_{yz} - i u_{xz}) \cos 2\theta + (u_{zz}/2 - u_{yy}/2 + i u_{xy}) \sin 2\theta}{\sqrt{6}} \\ \frac{(u_{yz} + i u_{xz}) \cos 2\theta + (u_{zz}/2 - u_{yy}/2 - i u_{xy}) \sin 2\theta}{\sqrt{6}} & \sqrt{\frac{2}{3}} (u_{xy} \cos 2\theta + u_{xz} \sin 2\theta) \\ 0 & \frac{(u_{yz} + i u_{xz}) \cos 2\theta + (u_{zz}/2 - u_{yy}/2 - i u_{xy}) \sin 2\theta}{\sqrt{2}} \end{pmatrix},$$

and the strain-tensor components $u_{\alpha\beta}$ are rewritten in the QW coordinate frame.

The dominant contribution to electron scattering is given by the terms proportional to u_{zz} because the out-of-plane component q_z of the wave vector of the phonon involved is typically much larger than the in-plane component $q_\|$. In this approximation, the matrix element of electron scattering from the state $(s,\boldsymbol{k})$ to the state $(s,\boldsymbol{k}')$, described by the wave functions (3), assisted by emission or absorption of a bulk acoustic phonon with the wave vector $\boldsymbol{q}$ has the form

$$V^{(\pm)}_{s\boldsymbol{k}',s\boldsymbol{k}} = \mp i \frac{q_z}{2} \left[\frac{\hbar N_{\boldsymbol{q}}^{(\pm)}}{2\rho\Omega_{\boldsymbol{q}}} \right]^{1/2} \left[\Xi_c Z_{11} + \Xi_v (Z_{44} + e^{is(\varphi' - \varphi)} Z_{33}) - \frac{i \sin 2\theta}{2\sqrt{2}} \Xi_{cv} (e^{is\varphi'} - e^{-is\varphi}) Z_{13} \right] \delta_{\boldsymbol{k}',\boldsymbol{k} \mp \boldsymbol{q}_\|}, \tag{7}$$

where $N_{\boldsymbol{q}}^{(\pm)} = N_{\boldsymbol{q}} + (1 \pm 1)/2$, $N_{\boldsymbol{q}}$ is the phonon occupation number, ρ is the crystal density, $\Omega_{\boldsymbol{q}} = c_s q$ is the phonon frequency, c_s is the speed of sound, $Z_{ij} = \int_{-\infty}^{+\infty} f_i(z) f_j(z) \exp(i q_z z) dz$, and $s =$ "$\pm$" is the index enumerating the Dirac cones. The matrix elements (7) contain asymmetric terms which are responsible for the emergence of oppositely directed electron fluxes $\boldsymbol{j}_s$ in the cones during the energy relaxation of heated electron gas.

To calculate the electron fluxes we introduce the electron distribution function $f_{s\boldsymbol{k}} = \bar{f}_{sk} + \delta f_{s\boldsymbol{k}}$, where $\bar{f}_{sk}$ is the quasiequilibrium function of the Fermi-Dirac type and $\delta f_{s\boldsymbol{k}}$ is the anisotropic part of the distribution function. It is assumed that the radiation absorption followed by electron-electron collisions forms the quasiequilibrium electron distribution with the electron temperature T_e which is slightly higher that the crystal lattice temperature T_0. The electron temperature can be found from the energy balance equation

$$\sum_{s,\boldsymbol{k},\boldsymbol{k}'} W^{(\mathrm{ph})}_{s\boldsymbol{k}',s\boldsymbol{k}} (\varepsilon_k - \varepsilon_{k'}) \bar{f}_{sk} (1 - \bar{f}_{sk'}) = I\eta, \tag{8}$$

where $W^{(\mathrm{ph})}_{s\boldsymbol{k}',s\boldsymbol{k}} = (2\pi/\hbar) \sum_{\boldsymbol{q},\pm} |V^{(\pm)}_{s\boldsymbol{k}',s\boldsymbol{k}}|^2 \delta(\varepsilon_{k'} - \varepsilon_k \pm \hbar\Omega_{\boldsymbol{q}})$ is the rate of electron scattering assisted by a phonon emission and absorption, scattering processes between states in different cones are neglected, I is the radiation intensity, and η is the free-carrier absorbance. The left-hand side of Eq. (8) describes the electron energy losses due to cooling by phonons while the right-hand side stands for the energy gain by the free-carrier absorption of radiation.

The electron fluxes are determined by the anisotropic part of the distribution function

$$\boldsymbol{j}_s = e \sum_{\boldsymbol{k}} \boldsymbol{v} \, \delta f_{s\boldsymbol{k}}, \tag{9}$$

where $\boldsymbol{v} = \nabla_{\boldsymbol{k}} \varepsilon / \hbar = v \, \boldsymbol{k}/k$ is the electron velocity. We consider that at low temperatures, relevant to the experimental conditions, the momentum relaxation of carriers is limited by elastic scattering from static defects while the energy relaxation is governed by deformation interaction with bulk acoustic phonons. Accordingly, $\delta f_{s\boldsymbol{k}}$ can be found from the Boltzmann equation

$$\frac{e}{c\hbar} [\boldsymbol{v} \times \boldsymbol{B}] \cdot \frac{d\, \delta f_{s\boldsymbol{k}}}{d\boldsymbol{k}} = \sum_{\boldsymbol{k}'} \left[W^{(\mathrm{ph})}_{s\boldsymbol{k},s\boldsymbol{k}'} \bar{f}_{sk'} (1 - \bar{f}_{sk}) - W^{(\mathrm{ph})}_{s\boldsymbol{k}',s\boldsymbol{k}} \bar{f}_{sk} (1 - \bar{f}_{sk'}) \right] - \frac{\delta f_{s\boldsymbol{k}}}{\tau_p}, \tag{10}$$

where τ_p is the momentum relaxation time. The straightforward calculation shows that the electron fluxes in the cones have the form

$$j_{\pm,x} = \mp \frac{ev \sin 2\theta}{2\sqrt{2}} \frac{n_\pm}{n} \left(\frac{d}{dE_{\mathrm{F}}} \frac{\omega_c \tau_p^2}{1 + (\omega_c \tau_p)^2} \right) \xi I \eta, \tag{11}$$

$$j_{\pm,y} = \mp \frac{ev \sin 2\theta}{2\sqrt{2}} \frac{n_\pm}{n} \left(\frac{d}{dE_{\mathrm{F}}} \frac{\tau_p}{1 + (\omega_c \tau_p)^2} \right) \xi I \eta, \tag{12}$$

where $n_\pm$ are the carrier densities in the cones, $n = n_+ + n_-$ is the total density, $\omega_c = eB_z v^2/(cE_{\mathrm{F}})$ is the cyclotron frequency, and

$$\xi = \frac{\int_{-\infty}^{+\infty} \Xi_{cv} Z_{13}(\Xi_c Z_{11} + \Xi_v Z_{33} + \Xi_v Z_{44}) q^2 dq}{\int_{-\infty}^{+\infty} [(\Xi_c Z_{11} + \Xi_v Z_{44})^2 + (\Xi_v Z_{33})^2] q^2 dq}.$$

Equations (11) and (12) are obtained assuming that $E_F \gg k_B T \gg \hbar\Omega_{\boldsymbol{q}}$ and $|n_+ - n_-| \ll n$.

The total electric current $\boldsymbol{j} = \boldsymbol{j}_+ + \boldsymbol{j}_-$ emerges due to an imbalance of the $\boldsymbol{j}_+$ and $\boldsymbol{j}_-$ contributions in the magnetic field. Assuming that the magnetic field splits the electron states due to the Zeeman effect but does not affect the scattering and taking into account that $\omega_c \tau_p \gg 1$, as in the experiment, we estimate the current magnitude

$$|\boldsymbol{j}| = \frac{ev \sin 2\theta}{2\sqrt{2} E_{\mathrm{F}} \omega_c} \frac{g\mu_0 B_z}{E_{\mathrm{F}}} \xi I \eta, \tag{13}$$

where g is the effective g factor and μ_0 is the Bohr magneton. For the circularly polarized radiation, the absorbance η in the vicinity of CR has the form

$$\eta = \frac{2e^2 E_{\mathrm{F}}}{c\hbar^2 n_\omega} \frac{\tau_p}{1 + (\omega - \omega_c)^2 \tau_p^2}, \tag{14}$$

where n_ω is the refractive index. The current j follows the spectral behavior of the absorbance η and exhibits a sharp peak at CR, whose position depends on the Fermi energy since $\omega_c \propto 1/E_{\mathrm{F}}$, in accordance with the experiment, see Fig. 2.

In the experimental setup we measure the voltage drop across a load resistor of 1 MΩ which is much higher than the sample resistance. The photovoltage induced in the open-circuit configuration at $\omega_c \tau_p \gg 1$ is given by

$$U = \left| j \frac{\omega_c \tau_p a}{\sigma} \right| \tag{15}$$

where a is the sample size and $\sigma = e^2 E_F \tau_p/(2\pi\hbar^2)$ is the conductivity at zero field. At a fixed radiation frequency, the dependence of photovoltage at CR on the carrier parameters is given by $U \propto g\tau_p/(\sqrt{n}\, v^2)$. The weak decrease of the peak voltage with the increases in the carrier density by an order of magnitude from p_1 to n_1 is observed in the experiment, see Fig. 2. The photovoltage is caused by the Zeeman splitting of electron states and, therefore, is an odd function of magnetic field and increases at CR much higher than does the radiation absorption. Thus, the above microscopic theory explains all major experimental observations. The theory suggests that the excited electric current is spin polarized. In the experiment we measure the voltage drop across the contacts caused by charge accumulation while the carrier spin state is not directly detected. The measurement of spin polarization of the photocurrent, e.g., by the optical means or ferroelectric contacts, is a challenging task to future.

V. SUMMARY

To summarize, we demonstrate that CR absorption by Dirac fermions in HgTe/HgCdTe QWs of critical thickness results in a resonant spin polarized electric current. The effect is very general and can be observed in other Dirac fermion systems with a strong spin-orbit coupling, e.g., surface states in 3D topological insulators like Bi_2Se_3 and Bi_2Te_3. For the latter case such a study is of special interest, because these crystals are centrosymmetric and, due to symmetry reasons, the photocurrent emerges only at surface layer. Consequently, it provides a unique selective access to fine details of their band structure like, e.g., effective mass and group velocity, as well as to the spin transport and spin-dependent scattering anisotropy.[58,59] Finally, large resonant currents detected at low magnetic fields, about 0.5 T for 2.5 THz, indicate that HgTe/HgCdTe QWs of critical thickness are a good candidate for frequency selective CR-assisted detectors similar to that based on photoconductivity in bulk InSb,[60] but operating at about 10 times lower magnetic fields.

ACKNOWLEDGMENTS

We acknowledge useful discussions with R. Winkler and E. G. Novik. The support from the DFG (SPP 1666), the Linkage Grant of IB of BMBF at DLR, RFBR, RF President Grants MD-2062.2012.2 and NSh-5442.2012.2, and the "Dynasty" Foundation is gratefully acknowledged.

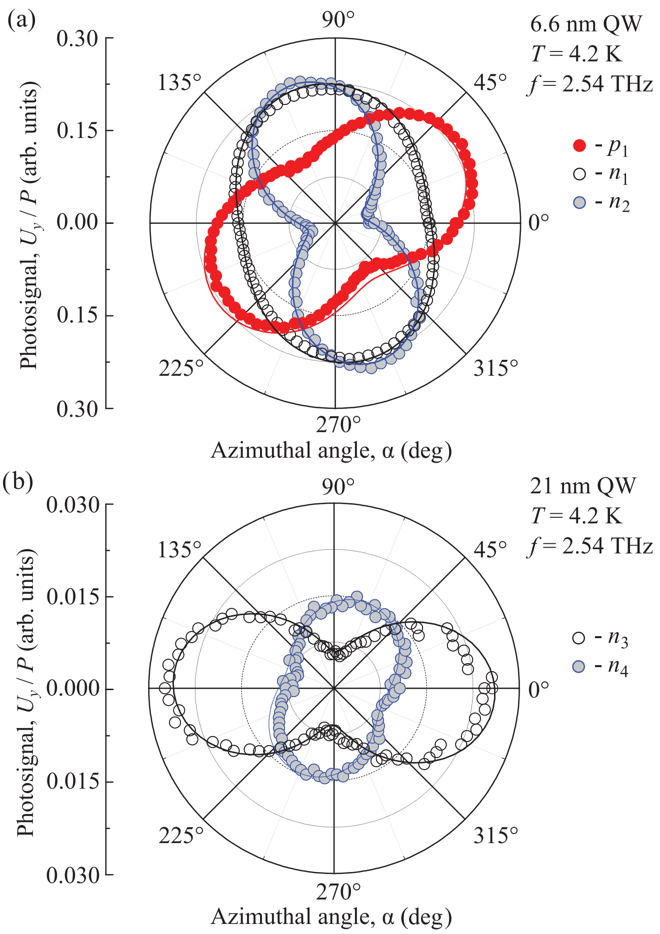

FIG. 6. (Color online) Polarization dependence of the photovoltage normalized by radiation power U_y/P excited with normal incident radiation in (a) 6.6 nm and (b) 21 nm QWs at zero magnetic field. The normalized photosignal is shown for different carrier densities and fitted after $U_y(\alpha)/P = A + B\sin(2\alpha) + C\cos(2\alpha)$.

APPENDIX: PHOTOGALVANIC EFFECTS AT ZERO MAGNETIC FIELD

Illuminating our (013)-oriented QW structures with normally incident THz radiation we observed a dc electric current even in the absence of magnetic field. Figures 6(a) and 6(b) show the dependence of the photosignal $U_y/P \propto j_y/P$ on the azimuth angle α measured for 6.6 and 21 nm QWs, respectively. Here α is the angle between the light polarization plane and the x direction. In both cases the data are well fitted by $U_y(\alpha)/P = A + B\sin(2\alpha) + C\cos(2\alpha)$. While in 6.6 nm QWs such a current has not been detected so far, in 21 nm QWs it was observed early in Ref. 40 and is demonstrated to be due to the photogalvanic effect.[61] Linear and circular photogalvanic effects for various spectral ranges have been studied in different III-V, II-VI, and SiGe quantum wells. Microscopic mechanisms of the photocurrent formation were widely discussed in the past, see, e.g., Refs. 37, 39, 47, and 62. We expect that similar mechanisms are also responsible for the zero-field current formation in HgTe/CdHgTe QWs. However, these mechanisms, in particular in QWs with the linear energy spectrum, require further analysis, which is out of the scope of the current paper. As it is shown in Ref. 40, a particular feature of the photogalvanic effect in QWs of (013)-orientation orientation is that, in contrast to (001)-grown QWs, it can be excited at normal incidence of radiation. Quantum wells grown on the (013)-oriented substrate belong to the trivial point group C_1 lacking any symmetry operation except the identity. Hence, symmetry does not impose any restriction on the relation between radiation electric field and photocurrent components. The polarization dependence of the photocurrent in structures of the C_1 point-group symmetry for the excitation along the QW normal with linearly polarized light is given by[40]

$$j_x = \left[\chi_{xxy}\sin 2\alpha - \frac{\chi_{xxx}+\chi_{xyy}}{2} + \frac{\chi_{xxx}-\chi_{xyy}}{2}\cos 2\alpha\right] I\eta, \tag{A1}$$

$$j_y = \left[\chi_{yxy}\sin 2\alpha - \frac{\chi_{yxx}+\chi_{yyy}}{2} + \frac{\chi_{yxx}-\chi_{yyy}}{2}\cos 2\alpha\right] I\eta, \tag{A2}$$

where $\boldsymbol{\chi}$ is the third rank photogalvanic tensor. Exactly this polarization dependence is observed in experiment, see Fig. 6. For C_1-symmetry group all components of the tensor $\boldsymbol{\chi}$ are linearly independent and may be nonzero. Consequently, even for a fixed light polarization, the CPGE photocurrent direction is not forced to a certain crystallographic axis. Moreover, it varies with temperature, radiation wavelength, etc.[40]

[1] M. Z. Hasan and C. L. Kane, Rev. Mod. Phys. **82**, 3045 (2010).

[2] J. E. Moore, Nature (London) **464**, 194 (2010).

[3] X.-L. Qi, S. C. Zhang, and X. L. Qi, Rev. Mod. Phys. **83**, 1057 (2011).

[4] A. H. Castro Neto, F. Guinea, N. M. R. Peres, K. S. Novoselov, and A. K. Geim, Rev. Mod. Phys. **81**, 109 (2009).

[5] B. A. Volkov and O. A. Pankratov, JETP Lett. **42**, 178 (1985).

[6] M. S. König, S. Wiedmann, C. Brüne, A. Roth, H. Buhmann, L. Molenkamp, X. L. Qi, and S. C. Zhang, Science **318**, 766 (2007).

[7] B. A. Bernevig, T. L. Hughes, and S. C. Zhang, Science **314**, 1757 (2006).

[8] B. Büttner, C. X. Liu, G. Tkachov, E. G. Novik, C. Brüne, H. Buhmann, E. M. Hankiewicz, P. Recher, B. Trauzettel, S. C. Zhang, and L. W. Molenkamp, Nat. Phys. **7**, 418 (2011).

[9] Z. D. Kvon, S. N. Danilov, D. A. Kozlov, C. Zoth, N. N. Mikhailov, S. A. Dvoretskii, and S. D. Ganichev, JETP Lett. **94**, 816 (2011).

[10] C. L. Kane and E. J. Mele, Phys. Rev. Lett. **95**, 146802 (2005).

[11] A. Roth, C. Brüne, H. Buhmann, L. W. Molenkamp, J. Maciejko, X. L. Qi, and S. C. Zhang, Science **325**, 294 (2009).

[12] D. Hsieh, D. Qian, L. Wray, Y. Xia, Y. S. Hor, R. J. Cava, and M. Z. Hasan, Nature (London) **452**, 970 (2008).

[13] C. Brüne, C. X. Liu, E. G. Novik, E. M. Hankiewicz, H. Buhmann, Y. L. Chen, X. L. Qi, Z. X. Shen, S. C. Zhang, and L. W. Molenkamp, Phys. Rev. Lett. **106**, 126803 (2011).

[14] X. L. Qi, T. L. Hughes, and S. C. Zhang, Phys. Rev. B **78**, 195424 (2008).

[15] A. M. Essin, J. E. Moore, and D. Vanderbilt, Phys. Rev. Lett. **102**, 146805 (2009).

[16] J. G. Checkelsky, Y. S. Hor, M. H. Liu, D. X. Qu, R. J. Cava, and N. P. Ong, Phys. Rev. Lett. **103**, 246601 (2009).

[17] H. L. Peng, K. J. Lai, D. S. Kong, S. Meister, Y. L. Chen, X. L. Qi, S. C. Zhang, Z. X. Shen, and Y. Cui, Nat. Mat. **9**, 225 (2010).

[18] J. Chen, H. J. Qin, F. Yang, J. Liu, T. Guan, F. M. Qu, G. H. Zhang, J. R. Shi, X. C. Xie, C. L. Yang, K. H. Wu, Y. Q. Li, and L. Lu, Phys. Rev. Lett. **105**, 176602 (2010).

[19] H. Z. Lu, J. Shi, and S. Q. Shen, Phys. Rev. Lett. **107**, 076801 (2011).

[20] M. H. Liu, J. S. Zhang, C. Z. Chang, Z. C. Zhang, X. Feng, K. Li, K. He, L. L. Wang, X. Chen, X. Dai, Z. Fang, Q. K. Xue, X. C. Ma, and Y. Y. Wang, Phys. Rev. Lett. **108**, 036805 (2012).

[21] D. A. Kozlov, Z. D. Kvon, N. N. Mikhailov, and S. A. Dvoretsky, JETP Lett. **96**, 730 (2012).

[22] P. Hosur, Phys. Rev. B **83**, 035309 (2011).

[23] B. Dora, J. Cayssol, F. Simon, and R. Moessner, Phys. Rev. Lett. **108**, 056602 (2012).

[24] Q. S. Wu, S. N. Zhang, Z. Fang, and X. Dai, Physica E **44**, 895 (2012).

[25] Y. G. Semenov, X. Li, and K. W. Kim, Phys. Rev. B **86**, 201401 (2012).

[26] J. W. McIver, D. Hsieh, S. G. Drapcho, D. H. Torchinsky, D. R. Gardner, Y. S. Lee, and N. Gedik, Phys. Rev. B **86**, 035327 (2012).

[27] T. Kitagawa, T. Oka, A. Brataas, L. Fu, and E. Demler, Phys. Rev. B **84**, 235108 (2011).

[28] N. H. Lindner, G. Refael, and V. Galitski, Nat. Phys. **7**, 490 (2011).

[29] D. Hsieh, J. W. McIver, D. H. Torchinsky, D. R. Gardner, Y. S. Lee, and N. Gedik, Phys. Rev. Lett. **106**, 057401 (2011).

[30] J. W. McIver, D. Hsieh, H. Steinberg, P. Jarillo-Herrero, and N. Gedik, Nat. Nanotech. **7**, 96 (2012).

[31] C. Kastl, T. Guan, X. Y. He, K. H. Wu, Y. Q. Li, and A. W. Holleitner, arXiv:1210.4743.

[32] Z. D. Kvon, E. B. Olshanetsky, N. N. Mikhailov, and D. A. Kozlov, Low Temp. Phys. **35**, 6 (2009).

[33] A. V. Ikonnikov, M. S. Zholudev, K. E. Spirin, A. A. Lastovkin, K. V. Maremyanin, V. Ya. Aleshkin, V. I. Gavrilenko, O. Drachenko, M. Helm, J. Wosnitza, M. Goiran, N. N. Mikhailov, S. A. Dvoretskii, F. Teppe, N. Diakonova, C. Consejo, B. Chenaud, and W. Knap, Semicond. Sci. Technol. **26**, 125011 (2011).

[34] M. S. Zholudev, A. V. Ikonnikov, F. Teppe, M. Orlita, K. V. Maremyanin, K. E. Spirin, V. I. Gavrilenko, W. Knap, S. A. Dvoretskiy, and N. N. Mihailov, Nanoscale Res. Lett. **7**, 534 (2012).

[35] Z. D. Kvon, S. N. Danilov, N. N. Mikhailov, S. A. Dvoretsky, and S. D. Ganichev, Physica E **40**, 1885 (2008).

[36] E. Ziemann, S. D. Ganichev, I. N. Yassievich, V. I. Perel, and W. Prettl, J. Appl. Phys. **87**, 3843 (2000).

[37] S. D. Ganichev, E. L. Ivchenko, and W. Prettl, Physica E **14**, 166 (2002).

[38] P. Schneider, J. Kainz, S. D. Ganichev, V. V. Bel'kov, S. N. Danilov, M. M. Glazov, L. E. Golub, U. Rssler, W. Wegscheider, D. Weiss, D. Schuh, and W. Prettl, J. Appl. Phys. **96**, 420 (2004).

[39] S. D. Ganichev and W. Prettl, *Intense Terahertz Excitation of Semiconductors* (Oxford University Press, Oxford, 2006).

[40] B. Wittmann, S. N. Danilov, V. V. Bel'kov, S. A. Tarasenko, E. G. Novik, H. Buhmann, C. Brüne, L. W. Molenkamp, E. L. Ivchenko, Z. D. Kvon, N. N. Mikhailov, S. A. Dvoretsky, N. Q. Vinh, A. F. G. van der Meer, B. Murdin, and S. D. Ganichev, Semicond. Sci. Technol. **25**, 095005 (2010).

[41] Our results reveal that for carrier densities p_1 [Fig. 1(a)] and n_1 (not shown) 2D system becomes fully quantized at low B_z so that R_{xy} approaches h/e^2 for B_z above 0.6 and 1.2 T for densities p_1 and n_1, respectively.

[42] The data contain small side peaks, which may originate from the spin-flip CR in QWs with strong spin-orbit coupling and Zeeman splitting.[44–46]

[43] J. R. Meyer, C. A. Hoffman, F. J. Bartoli, T. Wojtowicz, M. Dobrowolska, J. K. Furdyna, X. Chu, J. P. Faurie, and L. R. Ram-Mohan, J. Vac. Sci. Technol. B **10**, 1582 (1992).

[44] M. von Truchsess, V. Latussek, C. R. Becker, and E. Batke, J. Cryst. Growth **159**, 1104 (1996).

[45] M. Schultz, U. Merkt, A. Sonntag, U. Rössler, T. Colin, P. Helgesen, T. Skauli, and S. L, J. Cryst. Growth **184/185**, 1180 (1998).

[46] K. E. Spirin, A. V. Ikonnikov, A. A. Lastovkin, V. I. Gavrilenko, S. A. Dvoretskii, and N. N. Mikhailov, JETP Lett. **92**, 63 (2010).

[47] E. L. Ivchenko, *Optical Spectroscopy of Semiconductor Nanostructures* (Alpha Science, Harrow, UK, 2005).

[48] S. D. Ganichev, V. V. Bel'kov, S. A. Tarasenko, S. N. Danilov, S. Giglberger, Ch. Hoffmann, E. L. Ivchenko, D. Weiss, W. Wegscheider, Ch. Gerl, D. Schuh, J. Stahl, J. De Boeck, G. Borghs, and W. Prettl, Nat. Phys. **2**, 609 (2006).

[49] V. V. Bel'kov and S. D. Ganichev, Semicond. Sci. Technol. **23**, 114003 (2008).

[50] S. D. Ganichev, S. A. Tarasenko, V. V. Bel'kov, P. Olbrich, W. Eder, D. R. Yakovlev, V. Kolkovsky, W. Zaleszczyk, G. Karczewski, T. Wojtowicz, and D. Weiss, Phys. Rev. Lett. **102**, 156602 (2009).

[51] P. Olbrich, C. Zoth, P. Lutz, C. Drexler, V. V. Bel'kov, Ya. V. Terent'ev, S. A. Tarasenko, A. N. Semenov, S. V. Ivanov, D. R. Yakovlev, T. Wojtowicz, U. Wurstbauer, D. Schuh, and S. D. Ganichev, Phys. Rev. B **86**, 085310 (2012).

[52] M. I. Dyakonov, Ed., *Spin Physics in Semiconductors* (Springer, New York, 2008).

[53] (013)-grown QWs belong to the C_1 point group. Thus, the coupling between the components of $\boldsymbol{k}$ and spin vector is not predefined by symmetry.

[54] G. E. Pikus, V. A. Marushchak, and A. N. Titkov, Sov. Phys. Semicond. **22**, 115 (1988).

[55] E. L. Ivchenko and S. A. Tarasenko, JETP **99**, 379 (2004).

[56] S. A. Tarasenko, Semiconductors **42**, 967 (2008).

[57] G. L. Bir and G. E. Pikus, *Symmetry and Strain-Induced Effects in Semiconductors* (Wiley, New York, 1974).

[58] S. Giglberger, L. E. Golub, V. V. Bel'kov, S. N. Danilov, D. Schuh, Ch. Gerl, F. Rohlfing, J. Stahl, W. Wegscheider, D. Weiss, W. Prettl, and S. D. Ganichev, Phys. Rev. B **75**, 035327 (2007).

[59] M. Kohda, V. Lechner, Y. Kunihashi, T. Dollinger, P. Olbrich, C. Schönhuber, I. Caspers, V. V. Bel'kov, L. E. Golub, D. Weiss, K. Richter, J. Nitta, and S. D. Ganichev, Phys. Rev. B **86**, 081306 (2012).

[60] E. R. Brown, M. J. Wengler, and T. G. Phillips, J. Appl. Phys. **58**, 2051 (1985).

[61] Note that other microscopic roots of the photocurrent, such as, e.g., thermoelectricity, can be excluded because of (i) the polarization dependence of the photosignal and (ii) the spatial symmetry of the laser beam which is measured independently. The latter prevents the temperature gradient between contacts necessary for the thermoelectric effect.[63]

[62] E. L. Ivchenko and S. D. Ganichev, *Spin Photogalvanics* in *Spin Physics in Semiconductors*, edited by M. I. Dyakonov (Springer, New York, 2008).

[63] J. C. W. Song, M. S. Rudner, C. M. Marcus, and L. S. Levitov, Nano Lett. **11**, 4688 (2011).